LUND UNIVERSITY

RF EMF Exposure Compliance of mmWave Array Antennas for 5G User Equipment Application

Xu, Bo; Gustafsson, Mats; Shi, Shuai; Zhao, Kun; Ying, Zhinong; He, Sailing

2017

RF EMF Exposure Compliance of mmWave Array Antennas for 5G User Equipment Application

Bo Xu, Mats Gustafsson, Shuai Shi, Kun Zhao, Zhinong Ying, and Sailing He

Bo Xu
bxu@kth.se

Department of Electromagnetic Engineering
School of Electrical Engineering
KTH Royal Institute of Technology
Osquldas Väg 6
SE-100 44 Stockholm
Sweden

Mats Gustafsson
Mats.Gustafsson@eit.lth.se

Department of Electrical and Information Technology
Electromagnetic Theory
Lund University
P.O. Box 118
SE-221 00 Lund
Sweden

Shuai Shi
shuaishi@kth.se

Department of Electromagnetic Engineering
School of Electrical Engineering
KTH Royal Institute of Technology
Osquldas Väg 6
SE-100 44 Stockholm
Sweden

Kun Zhao
kunzhao@kth.se

Department of Electromagnetic Engineering
School of Electrical Engineering
KTH Royal Institute of Technology
Osquldas Väg 6
SE-100 44 Stockholm
Sweden

Zhinong Ying
Ying.Zhinong@sonymobile.com

Network Technology Lab
Research and Technology
Sony Mobile Communications
Mobilvägen
SE-221 88 Lund
Sweden

Sailing He
sailing@kth.se

Department of Electromagnetic Engineering
School of Electrical Engineering
KTH Royal Institute of Technology
Osquldas Väg 6
SE-100 44 Stockholm
Sweden

Abstract

In the millimeter-wave bands towards 5G, human exposure to radio frequency (RF) electromagnetic field (EMF) is evaluated in terms of free space power density, rather than specific absorption rate. Maximum power density emitted by 5G user equipment should not exceed the power density limits set by relevant regulatory guidelines. In this paper, we provide upper bounds of maximum power density of array antennas. When the total transmitted power of array antennas is constant, calculating the maximum power density of a particular averaging area can be solved by an eigenvalue decomposition. When the power output of each port is amplitude-constrained, the power density maximization problem can be relaxed to a semi-definite program. The maximum power density can be assessed by using different assessment methods. The maximum assessed power density can also be solved by an eigenvalue decomposition or a semi-definite relaxation. The results of maximum permissible transmitted power suggest that, for the ICNIRP limits, slight deviation is observed between different types of excitation conditions including unconstrained, uniform, and dynamic amplitudes; for the proposed FCC limits, more restrictive power constraints on each port can lead to higher maximum permissible transmitted power. We provide better methods than the traditional Monte Carlo method for RF EMF exposure compliance of 5G user equipment that contains array antennas with many possible excitations. The obtained results provide valuable insights for the standardization of RF EMF exposure compliance procedures of 5G user equipment.

1 Introduction

Millimeter-wave (mmWave) frequency bands contain large signal bandwidth and are very promising for the next-generation mobile communication, so called 5G, to reach data rate as high as $10\,\mathrm{Gb/s}$ and latency as low as $1\,\mathrm{ms}$ [2, 30]. In 2016, the U.S. Federal Communication Commission (FCC) formally allocated four new bands above $24\,\mathrm{GHz}$ towards 5G [12], among which the $27.5\text{-}28.35\,\mathrm{GHz}$ band is considered one of the most promising candidates for the first 5G commercial products [1, 15]. 5G user equipment (UE), such as smart phones and tablets, is required to comply with relevant regulatory guidelines, including the guidelines produced by the FCC [6, 7] and International Commission on Non-Ionizing Radiation Protection (ICNIRP) [20], constraining human exposure to radio frequency (RF) electromagnetic field (EMF). The IEEE also produces its own standard [18, 19], but it has not yet been adopted by any country.

Below the transition frequencies, which are $3\,\mathrm{GHz}$ for the IEEE, $6\,\mathrm{GHz}$ for ICNIRP, and $10\,\mathrm{GHz}$ for the FCC, the restriction metric of RF EMF exposure is defined in terms of specific absorption rate (SAR). SAR is a dosimetric metric of the rate at which energy is absorbed by the human body when exposed to RF EMF. A large number of studies on SAR for UE transmitting in existing cellular bands are available [3, 23, 24, 32, 38, 41, 45]. Because the correlation above the transition frequencies between SAR and the rising temperature of tissue is not as strong as

at lower frequencies, and the penetration depth of EMF into tissue decreases as the frequency increases [18, 20]. Therefore, free space power density becomes the pertinent restriction metric above the transition frequencies. The FCC, ICNIRP and IEEE stipulate that, instead of SAR measuring over a small sample volume of tissue, power density is explained as power flux density that is measured over a small sample area in free space. Recently, the FCC proposed a power density limit of $10\,\mathrm{W/m^2}$ for any averaging area of $1\,\mathrm{cm^2}$ above $6\,\mathrm{GHz}$ in order to be consistent with $1\,\mathrm{g}$ averaging (approximately $1\,\mathrm{cm^3}$) of SAR below $6\,\mathrm{GHz}$ [12, 26, 27]. This interpretation of power density is considered in this paper, although is has not yet formally become a part of administrative orders. Above $10\,\mathrm{GHz}$, ICNIRP specifies $10\,\mathrm{W/m^2}$ taken as an average over any $20\,\mathrm{cm^2}$ of exposed area, as the basic restriction for general public exposure. Additionally for ICNIRP, the maximum spatial power density averaged over any $1\,\mathrm{cm^2}$ shall not exceed $200\,\mathrm{W/m^2}$.

Such restrictions on RF EMF exposure determine the maximum permissible transmitted power of UE, constituting an important boundary condition for the design of mobile communication systems. Recently, a lot of works have been done regarding the RF EMF exposure of 5G UE. Colombi *et al.* [8] showed that the current regulations on RF EMF exposure lead to a non-physical discontinuity of 'several dB' in maximum permissible transmitted power because of the restriction metric switched from SAR to power density. Then Foster *et al.* [11] showed that the increase of maximum steady state temperature of human skin due to RF EMF exposure displays a similar discrepancy. Thors *et al.* [36] presented a systematic study of the maximum permissible transmitted power and maximum effective isotropic radiated power (EIRP) to comply with the guidelines specified by the ICNIRP, FCC, and IEEE for canonical dipole arrays. Zhao and Xu *et al.*[39, 40, 43] investigated the RF EMF exposure performance of 5G UE using different types of array antennas, and demonstrated that the maximum power density can possibly be assessed by using different compliance assessment methods.

In the mmWave bands, antenna dimensions are compact, so that array antennas can conceivably fit into UE. Array antennas can eliminate the frequency-dependent free space path loss and provide array gain to improve the link budget [2, 16, 28, 31, 35, 39, 40, 42, 43, 46]. Adaptive beam-forming arrays are probably a better choice for spatial diversity combining, reduction of impact of interference, and overcoming fading problems [13, 14]. The radiation patterns of such kind of arrays depend on the channel characteristics, UE orientations, and human body effect [35, 42, 44, 46]. Previous research on 5G RF EMF exposure [36, 39, 40, 43] is restricted to beam-steering arrays with a limited number of scan patterns using progressive phase-shift schemes. Adaptive beam-forming scenarios with an infinite number of possible excitations and radiation patterns have not been considered. In this paper, upper bounds of RF EMF exposure and the corresponding lower bounds of maximum permissible transmitted power levels are investigated regarding adaptive beam-forming scenarios. We demonstrate that the theoretical maximum power density and maximum assessed power density can be solved by an eigenvalue decomposition (EVD). When the power output of an individual element is constrained, the theoretical maximum power density and maximum assessed power density can be solved using
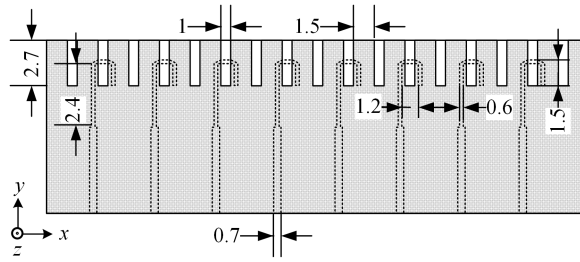
Figure 1: The configuration of the notch array operating at 28 GHz (unit: mm).

semi-definite relaxation (SDR). We provide solutions to the worst-case RF EMF exposure, and they can be used to state compliance of 5G UE using mmWave array antennas.

This paper is organized as follows. Section 2 briefly presents a 28 GHz 8×1 notch array used for RF EMF exposure studies. Section 3 shows that calculating the maximum power density of array antennas is an eigenvalue problem. Section 4 demonstrates that different kinds of power density assessment methods proposed in [39] are analyzed for array antennas using EVD. Section 5 presents a method of calculating maximum power density fed with amplitude-constrained excitations using SDR. Section 6 compares the maximum permissible transmitted power levels of different types of excitation schemes. The conclusion is in Section 7.

2 Array Antenna Configuration

Fig. 1 shows a 28 GHz 8×1 linear notch array printed on a Rogers RO4003 substrate (44 mm $\times$ 14 mm $\times$ 0.308 mm, $\epsilon_{\mathrm{r}} = 3.55$) designed for RF EMF exposure studies. The notch array is a potential candidate of 5G UE array antennas, because it can be placed at the edge of a Printed Circuit Board (PCB) and make good use of available space inside UE [16, 17, 35, 39, 40, 43]. The front side of the array is covered by metal with notches cut on the top. Parasitic notches are cut between adjacent radiating notches to reduce mutual coupling. The antennas are fed with 50 Ω microstrip lines on the back side (dashed lines), and the radiating notches are coupled-fed through bended microstrip lines. The array was simulated in the commercial full-wave simulation software CST MWS 2016. The electric and magnetic fields, induced by each element with the other elements matched, were exported from CST for further post-processing. The spatial sampling step width is 1 mm (0.093 λ_0) and the total number of sampling points is $145 \times 115 \times 102$. The total transmitted power level of the array, P_{total}, was scaled to 20 dBm, the same as the maximum permissible transmitted power level of Bluetooth Class 1 devices. In this paper, transmitted power is defined as the power output of the RF front end, and the excitation of the ith port, $w_i \in \mathbb{C}$, is defined as the output voltage of the corresponding RF front end, as they usually are the quantities known during UE antenna design.
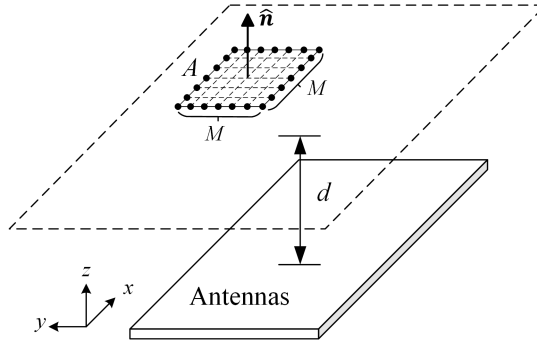
Figure 2: Illustration of the sampling scheme of fields at distance d in the $\hat{\boldsymbol{z}}$-direction.

3 RF EMF Exposure With Unconstrained Amplitudes

The power density of a specified averaging area A in a plane with a specified distance d away from the array antenna (for simplicity d is suppressed in the following equations) can be expressed as [36, 39, 40]

$$S^A = \frac{1}{2A} \iint_A \mathrm{Re} \left[\left(\sum_{i=1}^{N} w_i \boldsymbol{E}_i \right) \times \left(\sum_{i=1}^{N} w_i \boldsymbol{H}_i \right)^* \right] \cdot \hat{\boldsymbol{n}} \ \mathrm{d}A, \qquad (3.1)$$

where S^A denotes the area-averaged power density, the superscript $*$ denotes the complex conjugate, $\boldsymbol{E}_i$ and $\boldsymbol{H}_i$ are the field strengths excited by the ith port with others terminated with matched loads, $\hat{\boldsymbol{n}}$ denotes the unit vector perpendicular to the surface A. For the case with $\hat{\boldsymbol{n}} = \hat{\boldsymbol{z}}$, as shown in Fig. 2, (3.1) becomes

$$S^A = \frac{1}{2A} \iint_A \mathrm{Re} \left[\left(\sum_{i=1}^{N} w_i E_{ix} \right) \left(\sum_{i=1}^{N} w_i H_{iy} \right)^* - \left(\sum_{i=1}^{N} w_i E_{iy} \right) \left(\sum_{i=1}^{N} w_i H_{ix} \right)^* \right] \ \mathrm{d}A,$$
$$(3.2)$$

where E_{ix}, E_{iy}, H_{ix}, and H_{iy} denote the Cartesian components of the electric and magnetic fields. S^A for other $\hat{\boldsymbol{n}}$ directions can also be derived in similar ways. Although S^A can also be formulated in the cylindrical or spherical coordinate system, considering appearances of UE, like smart phones and tablets, here it is plausible to use the Cartesian coordinate system for our RF EMF exposure studies. We denote the weights of the array, $\boldsymbol{w} \in \mathbb{C}^{N \times 1}$, as

$$\boldsymbol{w} = [w_1, w_2, \ldots, w_N]^{\mathrm{T}}, \qquad (3.3)$$

where the superscript T denotes the transpose. We discretize the fields in the area A with $M \times M$ sampling points assuming A is square-shaped, as shown in Fig. 2. The electric and magnetic fields excited by each element at point (j, k) in A can be rewritten as

$$\begin{aligned} \boldsymbol{e}_{\tau jk} &= [E_{1\tau jk}, E_{2\tau jk}, \ldots, E_{N\tau jk}] \\ \boldsymbol{h}_{\tau jk} &= [H_{1\tau jk}, H_{2\tau jk}, \ldots, H_{N\tau jk}] \end{aligned} \qquad \tau = x, y, z, \qquad (3.4)$$
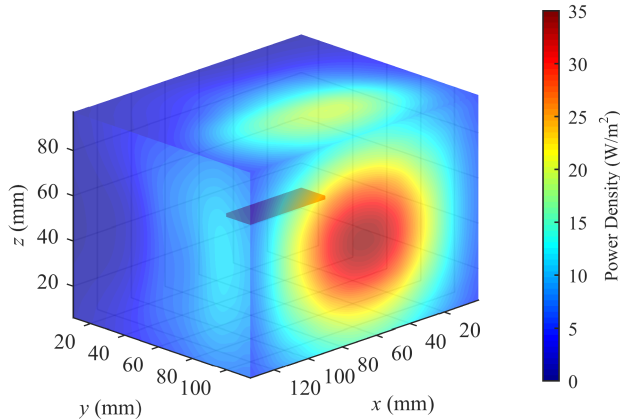
Figure 3: $S^A_{\max}$ distribution at $d = 45\,\mathrm{mm}$ away from the notch array, when $A = 1\,\mathrm{cm}^2$. Each pixel represents $S^A_{\max}$ of the corresponding averaging area A, where $S_{\max}$ occurs in the $\hat{\boldsymbol{y}}$-direction. The $S^A_{\max}$ distribution is almost symmetric about the $\hat{\boldsymbol{x}}$- and $\hat{\boldsymbol{z}}$-directions due to the symmetry of the array. Note that this figure is not an S^A distribution for a specific excitation.

where $\boldsymbol{e}_{\tau jk}, \boldsymbol{h}_{\tau jk} \in \mathbb{C}^{1 \times N}$, and $E_{i\tau jk}$ and $H_{i\tau jk}$ denote the Cartesian components of the electric and magnetic fields, respectively, produced by the ith port at (j, k). Then (3.2) can be expressed as

$$
\begin{aligned}
S^A &= \boldsymbol{w}^{\mathrm{H}} \left[\frac{1}{4M^2} \sum_{j=1}^{M} \sum_{k=1}^{M} \left(\mathbf{U}_{z^{(+)}jk} + \mathbf{U}^{\mathrm{H}}_{z^{(+)}jk} \right) \right] \boldsymbol{w} \\
&= \boldsymbol{w}^{\mathrm{H}} \mathbf{T}_{z^{(+)}} \boldsymbol{w},
\end{aligned}
\tag{3.5}
$$

where $\mathbf{U}_{z^{(+)}jk} = \boldsymbol{e}^{\mathrm{H}}_{xjk} \boldsymbol{h}_{yjk} - \boldsymbol{e}^{\mathrm{H}}_{yjk} \boldsymbol{h}_{xjk}$, and the superscript H denotes the conjugate transpose. In this paper, $M = 11$ for the FCC limits, and $M = 45$ for the ICNIRP limits. Note that the subscript $z^{(+)}$ in $\mathbf{U}_{z^{(+)}jk}$ denotes the sampling area in the $\hat{\boldsymbol{z}}$-direction of the array antenna. Other directions should also be considered in a similar manner, e.g. $\mathbf{U}_{x^{(-)}jk}$, etc. For simplicity, they are not shown here. Calculating the maximum power density of a particular area A, denoted as $S^A_{\max}$, can be formulated as

$$
\begin{aligned}
S^A_{\max} &= \max_{\boldsymbol{w} \in \mathbb{C}^{N \times 1}} \boldsymbol{w}^{\mathrm{H}} \mathbf{T} \boldsymbol{w} \\
&\text{subject to } \|\boldsymbol{w}\|^2 = \xi
\end{aligned}
\tag{3.6}
$$

where $\|\cdot\|$ denotes the norm, $\xi = 2P_{\mathrm{total}} Z_0$, and $Z_0 = 50\,\Omega$ is the input impedance of the RF front end. In (3.6), the subscript $z^{(+)}$ in $\mathbf{T}_{z^{(+)}}$ is omitted for simplicity, but keep in mind that $\mathbf{T}$ matrices in all the directions should be taken into account when calculating the maximum power density. As the only constraint in (3.6) is P_{total} and there is no extra constraint on the amplitude of an individual port, we denote (3.6) as the amplitude-unconstrained case, with respect to the amplitude-constrained cases in Section 5.
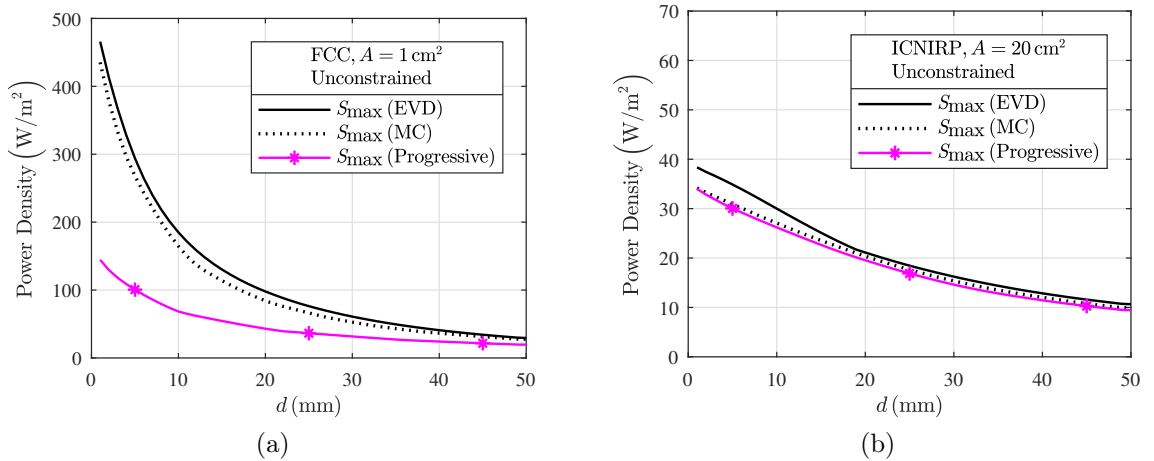
Figure 4: S_{max} calculated by using EVD, the MC method, and the progressive phase-shift scheme for the amplitude-unconstrained case, complying with (a) FCC limits and (b) ICNIRP limits.

Because (3.5) implies that $\mathbf{T} \in \mathbb{C}^{N \times N}$ is a Hermitian matrix whose eigenvalues are real [5], (3.6) can be solved by an eigenvalue decomposition (EVD) giving the exact solution of (3.6). S_{max}^{A}/ξ equals the largest eigenvalue of $\mathbf{T}$, and the complex weight of excitations is proportional to the corresponding eigenvector.

The maximum power density at a specified distance d should be the maximum power density of all the averaging areas with d away from the array in all directions, i.e. for $\pm\hat{\boldsymbol{x}}$, $\pm\hat{\boldsymbol{y}}$, and $\pm\hat{\boldsymbol{z}}$-directions and it can be written as

$$S_{\mathrm{max}} = \max_{\text{all } A} S_{\mathrm{max}}^{A}. \tag{3.7}$$

Fig. 3 presents an illustration of the S_{max}^{A} distribution for the distance $d = 45\,\mathrm{mm}$ away from the notch array and the averaging area $A = 1\,\mathrm{cm}^2$. Each pixel in the figure represents S_{max}^{A} of the corresponding averaging area A. The S_{max}^{A} distribution is almost symmetric about the $\hat{\boldsymbol{x}}$- and $\hat{\boldsymbol{z}}$-directions due to the symmetry of the array. Observe that Fig. 3 is not a power density distribution for a particular excitation, but the S_{max}^{A} distribution concerning all the possible excitations when only P_{total} is kept constant. It shows that, at $d = 45\,\mathrm{mm}$, S_{max} occurs in the $\hat{\boldsymbol{y}}$-direction. S_{max} represents the worst-case scenario of RF EMF exposure, and would be used to state compliance and calculate the maximum permissible transmitted power levels.

A Monte Carlo (MC) method was applied to $\boldsymbol{w}$ with 100,000 random inputs to verify the previous derivations. The comparison of results of EVD and the MC method are shown in Fig. 4, together with the results produced by the progressive phase-shift scheme employed in [36, 39, 40, 43]. The progressive phase-shift angle between adjacent elements changes from $-180°$ to $180°$ for every $30°$. As shown in the figure, on the one hand, EVD does give the theoretical upper bound of RF EMF exposure for any possible excitation, on the other hand, the progressive phase-shift scheme underestimates the worst-case exposure. The progressive phase-shift

scheme might not be used to state compliance for the case with an infinite number of possible excitations.

It is noteworthy that ICNIRP does not stipulate the minimum compliance distance, above which power density should be lower than the power density limits $10\,\mathrm{W/m}^2$. The FCC stipulated that compliance measurements and calculations should be made at a minimum distance of $5\,\mathrm{cm}$ from the radiating source [7]. However, the FCC noticed that, for UE operating close to human bodies, such requirement on the minimum compliance distance does not make sense, and proposed to remove it [27]. In order to state compliance with the power density limits at distance d, compliance must also be ensured for all distances larger than or equal to d, especially for array antennas, where the maximum power density may occur some distance away due to the focusing of energy [36]. Same phenomenon can be observed in Fig. 6(a) where S_max increases slightly from $d = 1\,\mathrm{mm}$ to $d = 2\,\mathrm{mm}$.

4   Power Density Assessment Methods

The previous work [40] demonstrated that S_max can possibly be assessed through plane-wave equivalent power density, because measuring both fields would add complexity to the measurement set-up and increase the measurement time. The plane-wave equivalent power density of array antennas can be expressed as [40]

$$S_\mathrm{PW}^A = \frac{1}{2\eta_0 A} \iint_a \left| \sum_{i=1}^{N} w_i \boldsymbol{E}_i \right|^2 \, \mathrm{d}A, \tag{4.1}$$

or

$$S_\mathrm{PW,t}^A = \frac{1}{2\eta_0 A} \iint_A \left| \sum_{i=1}^{N} w_i \boldsymbol{E}_{i,\mathrm{t}} \right|^2 \, \mathrm{d}A, \tag{4.2}$$

where η_0 denotes the free space impedance, and $\boldsymbol{E}_{i,\mathrm{t}}$ denotes the tangential component of the electric field.

With knowledge of the magnitude of the electric fields of each antenna element, conservative field combining methods have been developed for multi-port antennas, including the magnitude field combining method (MFCM) and the components field combining method (CFCM) [10, 29, 37]. They are suitable for use in combination with scalar measurement systems, yet [40] suggested that they may have the conservativeness problem, i.e. they would overestimate the maximum power density, when using the progressive phase-shift scheme. MFCM and CFCM for array antennas can be expressed as [10, 29, 37, 40]

$$S_\mathrm{MFCM}^A = \frac{1}{2\eta_0 A} \iint_A \left(\sum_{i=1}^{N} |w_i| \, |\boldsymbol{E}_i| \right)^2 \, \mathrm{d}A, \tag{4.3}$$

and

$$S_\mathrm{CFCM}^A = \frac{1}{2\eta_0 A} \iint_A \sum_{\tau=x,y,z} \left(\sum_{i=1}^{N} |w_i| \, |E_{i\tau}| \right)^2 \, \mathrm{d}A. \tag{4.4}$$
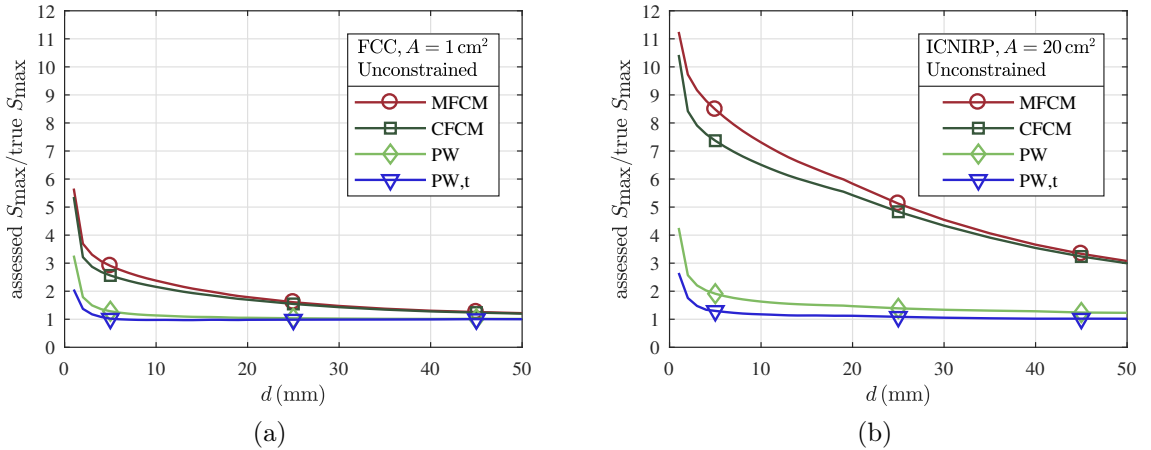
Figure 5: The ratio of the assessed $S_{\max}$ to the true $S_{\max}$, complying with (a) FCC limits and (b) ICNIRP limits
.

In fact, the assessed $S_{\max}^A$ of (4.1)-(4.4) for a particular area A can be expressed in a similar manner as the eigenvalue problem (3.6), and can be solved in the same way. The corresponding assessed $S_{\max}$ is denoted as $S_{\mathrm{PW,max}}$, $S_{\mathrm{PWt,max}}$, $S_{\mathrm{MFCM,max}}$, and $S_{\mathrm{CFCM,max}}$, respectively. Their corresponding $\mathbf{T}$ matrices are listed in Appendix. Fig. 5 shows the comparison of the true and assessed $S_{\max}$ against distance d by using EVD. It shows that MFCM and CFCM are not suitable for the power density assessment, since $S_{\mathrm{MFCM,max}}$ and $S_{\mathrm{CFCM,max}}$ are several times higher than $S_{\max}$ in the proximity of array antennas. $S_{\mathrm{PW,max}}$ and $S_{\mathrm{PWt,max}}$ are more suitable, and $S_{\mathrm{PWt,max}}$ shows better assessment results than $S_{\mathrm{PW,max}}$, although it still has considerable deviation when $d < 5\,\mathrm{mm}$. Comparing Fig. 5(a) with Fig. 5(b), generally, the assessment methods are more suitable for the FCC limits with smaller averaging area A than for the ICNIRP limits with greater A, on par with the results using the progressive phase-shift scheme at $15\,\mathrm{GHz}$ in [40]. Note that, according to the regulatory guidelines, the assessment results are neither necessary nor sufficient for calculating or measuring the true $S_{\max}$. They are just reference values for manufacturers, operators, and regulators to determine whether the power density limits are likely to be exceeded [6, 20].

5 RF EMF Exposure with Constrained Amplitudes

In the previous sections, we assumed that the amplitudes of all ports are variable and unconstrained, except that P_{total} remains constant. The extreme situation is that all the energy is transmitted through a single port. [36, 43] demonstrated that $S_{\max}$ increases as the number of radiating elements decreases, because the localized energy is confined in a smaller area. In the real world, the transmitted power of each port could be limited due to the output constraint of power amplifiers in the RF front end. In other words, the maximum transmitted power of each port could
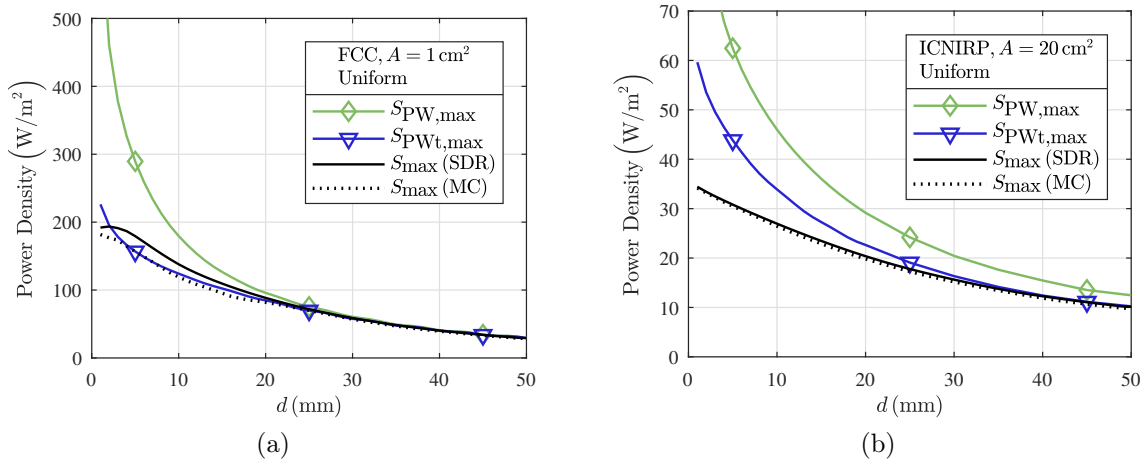
Figure 6: Comparison of $S_{\max}$ produced by SDR and MC method, together with $S_{\mathrm{PW,max}}$ and $S_{\mathrm{PWt,max}}$ calculated by SDR, when $|w_i|^2 = \zeta$, complying with (a) FCC limits, (b) ICNIRP limits.

be lower than P_{total}.

5.1 Uniform Amplitudes

First, we consider the case that the amplitudes of all ports are uniform. The power density maximization problem can be formulated as

$$
\begin{aligned}
S_{\max}^A = \max_{\boldsymbol{w} \in \mathbb{C}^{N \times 1}} \ & \boldsymbol{w}^{\mathrm{H}} \mathbf{T} \boldsymbol{w} \\
\text{subject to } & |w_i|^2 = \zeta, \ i = 1, 2, \ldots, N,
\end{aligned}
\tag{5.1}
$$

where $\zeta = 2P_{\mathrm{total}} Z_0 / N$. This problem is known as a complex quadratic optimization problem, which can be relaxed to a semi-definite program (SDP) [4, 21, 25, 33, 34] by using $\boldsymbol{w}^{\mathrm{H}} \mathbf{T} \boldsymbol{w} = \mathrm{Tr}(\mathbf{T} \boldsymbol{w} \boldsymbol{w}^{\mathrm{H}}) = \mathrm{Tr}(\mathbf{T} \mathbf{W})$ and dropping the constraint $\mathrm{rank}(\mathbf{W}) = 1$:

$$
\begin{aligned}
\widetilde{S}_{\max}^A = \max_{\mathbf{W} \in \mathbb{C}^{N \times N}} \ & \mathrm{Tr}(\mathbf{T} \mathbf{W}) \\
\text{subject to } & \mathrm{W}_{ii} = \zeta, \ i = 1, 2, \ldots, N \\
& \mathbf{W} \succeq 0.
\end{aligned}
\tag{5.2}
$$

SDP (5.2) can be solved by MATLAB toolbox CVX [9]. Let the optimal solution of SDP (5.2) be $\widetilde{\mathbf{W}}$. Generally for SDP, if $\widetilde{\mathbf{W}}$ is of rank one, then naturally $S_{\max}^A = \widetilde{S}_{\max}^A$, and we can write $\widetilde{\mathbf{W}} = \widetilde{\boldsymbol{w}} \widetilde{\boldsymbol{w}}^{\mathrm{H}}$, where $\widetilde{\boldsymbol{w}}$ is the corresponding semi-definite relaxed (SDR) solution of the original problem (5.1). If $\widetilde{\mathbf{W}}$ is not of rank one, we can still derive the approximate optimal solution $\widetilde{\boldsymbol{w}}_{\mathrm{a}}$ from $\widetilde{\mathbf{W}}$ [21, 25, 33]. Specifically, [22] demonstrated that there exists a solution of rank one for SDP (5.2). If the optimal solution $\widetilde{\mathbf{W}}$ is not of rank one, it still has the same $\widetilde{S}_{\max}^A$ as the solution of rank one gives. In other words, we can always obtain the exact solution of the original problem (5.1) from SDP (5.2).
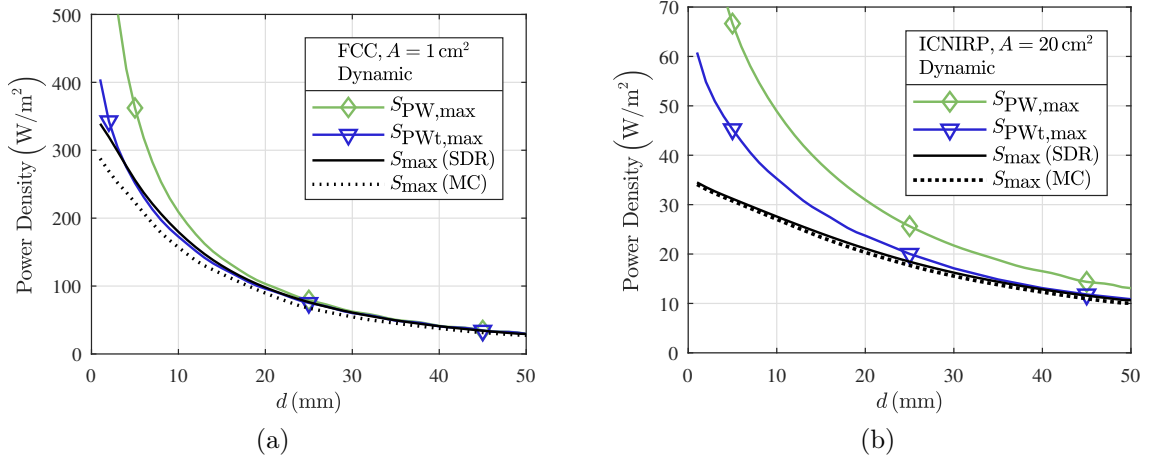
Figure 7: Comparison of $S_{\max}$ produced by SDR and MC method, together with $S_{\mathrm{PW,max}}$ and $S_{\mathrm{PWt,max}}$ calculated by SDR, when $|w_i|^2 \leq \zeta_{\mathrm{ub}}$, complying with (a) FCC limits, (b) ICNIRP limits.

Because different types of assessed $S_{\max}^A$ presented in Section IV can be derived in the same format as (5.1) for the amplitude-uniform case by using the $\mathbf{T}$ matrices listed in the Appendix, they can also be relaxed to SDP. The MC method was applied to $\boldsymbol{w}$ with 100,000 random inputs to the original problem (5.1) to verify the validity of SDR. Fig. 6 compares the $S_{\max}$ produced by SDR to the results produced by the MC method, together with the $S_{\mathrm{PW,max}}$ and $S_{\mathrm{PWt,max}}$ calculated using SDR. In Fig. 6, similar trends as in Fig. 5 are observed, i.e. $S_{\mathrm{PWt,max}}$ shows better agreement with $S_{\max}$ than $S_{\mathrm{PW,max}}$, and the assessment methods are more suitable for the FCC limits than for the ICNIRP limits. The $S_{\max}$ produced by SDR is as expected higher than the results produced by the MC method. However, an apparent discrepancy between the results of SDR and the MC method can be observed in Fig. 6(a), as well as in Fig. 7(a). To verify the validity of SDR, $\widetilde{\boldsymbol{w}}$ or $\widetilde{\boldsymbol{w}}_{\mathrm{a}}$ obtained by SDR is substituted into the original problem (5.1), and this procedure gives the same results as SDP (5.2) gives (not shown in the figure). Thus the SDR successfully provides the upper bound. The discrepancy could be attribute to that the number of random inputs of the MC method may not be large enough, or there might be in nature very few possible excitations that could approach the upper bound. Same kind of verification is also applied in Section 5.2.

5.2 Dynamic Amplitudes

Here, we consider the more complicated case that the amplitude of each port is constrained within a dynamic range, i.e. $|w_i|^2/2Z_0 \leq P_{\mathrm{ub}}$, while P_{total} remains
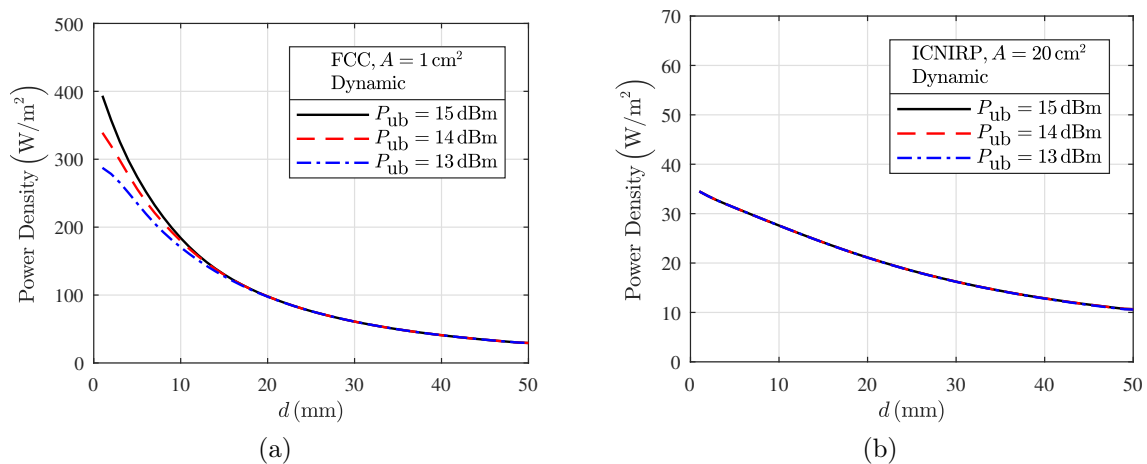
Figure 8: Comparison of $S_{\max}$ produced by SDR, when the transmitted power of each port is at most $13\,\mathrm{dBm}$, $14\,\mathrm{dBm}$, and $15\,\mathrm{dBm}$, respectively, complying with (a) FCC limits, (b) ICNIRP limits.

constant. The maximization problem can be formulated as

$$
\begin{aligned}
S_{\max}^{A} = \max_{\boldsymbol{w} \in \mathbb{C}^{N \times 1}} & \ \boldsymbol{w}^{\mathrm{H}} \mathbf{T} \boldsymbol{w} \\
\text{subject to } & |w_i|^2 \leq \zeta_{\mathrm{ub}}, \ i = 1, 2, \ldots, N \\
& \|\boldsymbol{w}\|^2 = \xi,
\end{aligned}
\tag{5.3}
$$

where $\zeta_{\mathrm{ub}} = 2 P_{\mathrm{ub}} Z_0$. Such a complex quadratic optimization problem can also be relaxed to SDP:

$$
\begin{aligned}
\widetilde{S}_{\max}^{A} = \max_{\mathbf{W} \in \mathbb{C}^{N \times N}} & \ \mathrm{Tr}\left(\mathbf{T}\mathbf{W}\right) \\
\text{subject to } & \mathrm{W}_{ii} \leq \zeta_{\mathrm{ub}}, \ i = 1, 2, \ldots, N \\
& \mathrm{Tr}\left(\mathbf{W}\right) = \xi \\
& \mathbf{W} \succeq 0.
\end{aligned}
\tag{5.4}
$$

A similar procedure is used to solve SDP (5.4) as solving SDP (5.2), except that there might not exist a solution of rank one as in SDP (5.2). But we are still able to derive $\widetilde{\boldsymbol{w}}_{\mathrm{a}}$ and $\widetilde{S}_{\max}^{A}$ as stated previously. In Fig. 7, the results produced by SDP (5.4) are as expected little higher than the results produced by the MC method when $P_{\mathrm{ub}} = 14\,\mathrm{dBm}$. The $S_{\mathrm{PW,max}}$ and $S_{\mathrm{PWt,max}}$ have the same behavior as in Fig. 5 and Fig. 6. Fig. 8 depicts the comparison of $S_{\max}$ for different P_{ub}. It shows that, for lower P_{ub}, the resulting $S_{\max}$ is also lower when d is small, especially for the FCC limits. This is because if P_{ub} is large, most of the energy will be transmitted through one or a few ports. This leads to higher $S_{\max}$ [36, 43]. As P_{ub} decreases from $15\,\mathrm{dBm}$ to $13\,\mathrm{dBm}$, excessive power will be reallocated to other ports due to the power constraint. One extreme situation is that $P_{\mathrm{ub}} = 20\,\mathrm{dBm}$, the same as the amplitude-unconstrained case (3.6), whose $S_{\max}$ shown in Fig. 4(a) is much higher than the result presented in Fig. 8(a). The other extreme situation is $P_{\mathrm{ub}} = 11\,\mathrm{dBm}$, the same as the amplitude-uniform case (5.1), whose $S_{\max}$ shown in Fig. 6(a) is lower
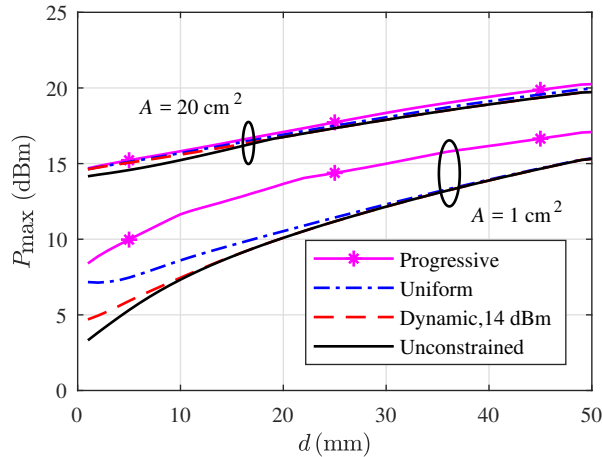
Figure 9: $P_{\max}$ of the notch array excited with unconstrained amplitudes, uniform amplitudes, and dynamic amplitudes ($P_{\mathrm{ub}} = 14\,\mathrm{dBm}$), along with the progressive phase-shift scheme.

than the result presented in Fig. 8(a). For the ICNIRP limits, such trend still exists, but the difference between different levels of P_{ub} is inconspicuous. This is because the 'length' of the $\mathbf{T}$ matrices for a large averaging area A does not vary as drastically as for a small A.

6   Maximum Permissible Transmitted Power

In the previous sections, $S_{\max}$ under different excitation conditions are calculated for $P_{\mathrm{total}} = 20\,\mathrm{dBm}$. In order to state compliance with the power density limits $S_{\mathrm{lim}} = 10\,\mathrm{W/m^2}$ at a specified distance d, compliance must also be ensured for all the distances $d' \geq d$. The corresponding maximum permissible transmitted power, $P_{\max}$, can be determined by

$$\frac{P_{\max}(d)}{S_{\mathrm{lim}}} = \frac{P_{\mathrm{total}}}{\max_{d' \geq d} S_{\max}(d')}. \tag{6.1}$$

Fig. 9 shows $P_{\max}$ against d, when amplitudes are unconstrained, uniform, dynamic, along with using the progress phase-shift scheme. Generally, the $P_{\max}$ complying with the ICNIRP limits are higher than the $P_{\max}$ complying with the FCC limits, the same as in [8, 36, 39, 40]. The $P_{\max}$ complying with the ICNIRP limits produced by different excitation schemes do not have much difference ($< 0.7\,\mathrm{dB}$). However, significant difference can be observed for the FCC limits. The $P_{\max}$ found in [36, 39, 40, 43] using progressive phase-shift schemes may be overestimated by several dB for $A = 1\,\mathrm{cm^2}$. More restrictive constraints on the amplitudes lead to a lower $S_{\max}$ as mentioned before, and results in the higher corresponding $P_{\max}$. The progressive phase-shift scheme is the most restrictive constraint comprised of uniform amplitudes and limited choices of excitation phases. The amplitude-uniform case has the second highest $P_{\max}$, although it is very hard to identify for the ICNIRP limits. The amplitude-unconstrained case (although strictly speaking, it is

still constrained by P_{total}) has the least power constraint on an individual element, therefore its P_{max} is always the most conservative for both regulatory limits.

For UE to be used in the immediate vicinity of the human body, the power density limits result in P_{max} significantly below what is specified for existing 4G communication (23-24 dBm), in line with the findings in [8, 36, 39, 40, 43]. Approaches to increase the P_{max} levels presented in the previous publications include increasing the number of antenna elements, choosing low frequency bands like 15 GHz [36, 43], and choosing omni-directional types of antenna elements [39]. This paper implies that, another way to increase P_{max} levels is to select a limited number of excitations as a code book of transmission modes, especially for UE to be compliant with the FCC limits. Such selection of code books needs extra knowledge of statistical channel state information. Compromise between the link budget and RF EMF exposure compliance should be reached, however, this is beyond the scope of this paper.

7 Conclusion

For array antennas, RF EMF exposure performance will vary with the array excitation. As a consequence, compliance with RF EMF exposure limits needs to be verified for all possible excitations. In this paper, the problems are formulated in complex quadratic forms, and the methods of obtaining theoretical upper bounds of RF EMF exposure for all possible excitations are investigated. The methods can be used for calculating RF EMF exposure of 5G UE using array antennas, and potentially provide guidelines of antenna design to be compliant with the regulatory limits. By using a 28 GHz 8×1 notch array as an example, the obtained results provide valuable insights for the RF EMF exposure performance of 5G UE and for the standardization of RF EMF exposure compliance of 5G UE in the future.

We demonstrated that the maximum power density can be solved by EVD when the amplitude of each port is unconstrained while the total transmitted power is kept unchanged. The results produced by EVD agree well with the results from the MC method.

When considering more realistic cases that the power output of an individual element is constrained, the calculations of maximum power density and maximum assessed power density can be solved by SDR. The results show that, more restrictive power constraint put on the output of individual element, the lower upper bound of RF EMF exposure obtained, especially for the FCC limits.

We showed that different types of maximum assessed power density can also be solved by EVD or SDR. The results show that MFCM and CFCM are too conservative for RF EMF exposure assessment. Plane-wave equivalent power density based on the tangential components of the electric fields is shown to be a more proper assessment methods, although some deviation cannot be ignored in the proximity of array antennas.

As a result, for the ICNIRP limits, different types of excitation schemes do not have much difference on the maximum permissible transmitted power levels. For the FCC limits, choosing different power constraints of each port could lead to significant

14

differences on the maximum permissible transmitted power levels.

Appendix

Assuming $\hat{\boldsymbol{n}} = \hat{\boldsymbol{z}}$, the $\mathbf{T}_{z(+)}$ matrices of (4.1) and (4.2) can be written as

$$\mathbf{T}_{z(+)\mathrm{PW}} = \frac{1}{2\eta_0 M^2} \sum_{j=1}^{M} \sum_{k=1}^{M} \sum_{\tau=x,y,z} \boldsymbol{e}_{\tau jk}^{\mathrm{H}} \boldsymbol{e}_{\tau jk}, \tag{7.1}$$

and

$$\mathbf{T}_{z(+)\mathrm{PW,t}} = \frac{1}{2\eta_0 M^2} \sum_{j=1}^{M} \sum_{k=1}^{M} \left(\boldsymbol{e}_{xjk}^{\mathrm{H}} \boldsymbol{e}_{xjk} + \boldsymbol{e}_{yjk}^{\mathrm{H}} \boldsymbol{e}_{yjk} \right). \tag{7.2}$$

The magnitude of the electric fields excited by each port can be rewritten as

$$\boldsymbol{e}_{jk}^{(\mathrm{m})} = \left[|\boldsymbol{E}_{1jk}|, |\boldsymbol{E}_{2jk}|, \ldots, |\boldsymbol{E}_{Njk}| \right], \tag{7.3}$$

where $\boldsymbol{e}_{jk}^{(\mathrm{m})} \in \mathbb{R}^{1 \times N}$, the superscript (m) denotes the magnitude, and $|\boldsymbol{E}_{ijk}|$ denotes the magnitude of the electric fields excited by the ith port. The corresponding $\mathbf{T}_{z(+)}$ matrix of (4.3) is

$$\mathbf{T}_{z(+)\mathrm{MFCM}} = \frac{1}{2\eta_0 M^2} \sum_{j=1}^{M} \sum_{k=1}^{M} \boldsymbol{e}_{jk}^{(\mathrm{m})\mathrm{H}} \boldsymbol{e}_{jk}^{(\mathrm{m})}. \tag{7.4}$$

The magnitude of the Cartesian components of the electric fields excited by each port can be rewritten as

$$\boldsymbol{e}_{\tau jk}^{(\mathrm{m})} = \left[|E_{1\tau jk}|, |E_{2\tau jk}|, \ldots, |E_{N\tau jk}| \right], \ \tau = x, y, z, \tag{7.5}$$

where $\boldsymbol{e}_{\tau jk}^{(\mathrm{m})} \in \mathbb{R}^{1 \times N}$. Then the $\mathbf{T}_{z(+)}$ matrix of (4.4) can be written as

$$\mathbf{T}_{z(+)\mathrm{CFCM}} = \frac{1}{2\eta_0 M^2} \sum_{j=1}^{M} \sum_{k=1}^{M} \sum_{\tau=x,y,z} \boldsymbol{e}_{\tau jk}^{(\mathrm{m})\mathrm{H}} \boldsymbol{e}_{\tau jk}^{(\mathrm{m})}. \tag{7.6}$$

By substituting these $\mathbf{T}$ matrics into (3.6), (5.1), or (5.3), considering all the Cartesian directions, the assessed $S_{\max}^A$ can be derived by solving EVD or SDR.

Acknowledgment

References

[1]   *5G Radio Access*. White Paper. Ericsson, 2016.

[2]   J. G. Andrews, S. Buzzi, W. Choi, S. V. Hanly, A. Lozano, A. C. K. Soong, and J. C. Zhang. "What will 5G be?" *IEEE J. Sel. Areas Commun.* 32 (6) (2014): pp. 1065–1082.

[3]   B. B. Beard, W. Kainz, T. Onishi, T. Iyama, S. Watanabe, O. Fujiwara, J. Wang, G. Bit-Babik, A. Faraone, J. Wiart, A. Christ, N. Kuster, A.-K. Lee, H. Kroeze, M. Siegbahn, J. Keshvari, H. Abrishamkar, W. Simon, D. Manteuffel, and N. Nikoloski. "Comparisons of computed mobile phone induced SAR in the SAM phantom to that in anatomically correct models of the human head". *IEEE Transactions on Electromagnetic Compatibility* 48 (2) (2006): pp. 397–407.

[4]   S. Boyd and L. Vandenberghe. "Convex Optimization". Cambridge University Press, 2004.

[5]   J. B. Carrell. "Fundamentals of Linear Algebra". 2005.

[6]   *Code of Federal Regulations, title 47, part 1.1310*. FCC, 2016.

[7]   *Code of Federal Regulations, title 47, part 2.1093*. FCC, 2016.

[8]   D. Colombi, B. Thors, and C. Törnevik. "Implications of EMF exposure limits on output power levels for 5G devices above 6 GHz". *IEEE Antennas and Wireless Propagation Letters* 14 (2015): pp. 1247–1249.

[9]   *CVX: MATLAB software for disciplined convex programming, version 2.1*. URL: http://cvxr.com/cvx/download/.

[10] A. Faraone, H. Heinrich, T. Harrington, J. Keshvari, T. Onishi, J.-K. Pack, J. Pledl, J. Prats, M. Wood, and P. Zollman. *Guidance for evaluating exposure from multiple electromagnetic sourcesGuidance for evaluating exposure from multiple electromagnetic sources*. Tech. rep. IEC TR 62630:2010. International Electrotechnical Commission, 2010.

[11] K. Foster and D. Colombi. "Thermal response of tissue to RF exposure from canonical dipoles at frequencies for future mobile communication systems". *Electron. Lett.* 53 (5) (2017): pp. 360–362.

[12] *Further notice of proposed rulemaking*. Commission Documents 16-89. FCC, 2016.

[13] L. C. Godara. "Application of antenna arrays to mobile communications. II. beam-forming and direction-of-arrival considerations". *Proceedings of the IEEE* 85 (8) (1997): pp. 1195–1245.

[14] L. C. Godara. "Applications of antenna arrays to mobile communications. I. performance improvement, feasibility, and system considerations". *Proceedings of the IEEE* 85 (7) (1997): pp. 1031–1060.

[15] *Heavy Reading Whitepaper: Exploring the potential of mmWave for 5G mobile access*. White Paper. Qualcomm, 2016.

[16]   J. Helander, K. Zhao, Z. Ying, and D. Sjöberg. "Performance analysis of millimeter-wave phased array antennas in cellular handsets". *IEEE Antennas and Wireless Propagation Letters* 15 (2016): pp. 504–507.

[17]   J. Helander and Z. Ying. "Stripline Coupled Antenna with Periodic Slots for Wireless Electronic Devices". Pat. WO2016072035. 2016.

[18]   *IEEE Standard for Safety Levels with Respect to Human Exposure to Radio Frequency Electromagnetic Fields, 3 kHz to 300 GHz.* IEEE, 2006.

[19]   *IEEE Standard for Safety Levels with Respect to Human Exposure to Radio Frequency Electromagnetic Fields, 3 kHz to 300 GHz Amendment 1: Specifies Ceiling Limits for Induced and Contact Current, Clarifies Distinctions between Localized Exposure and Spatial Peak Power Density.* IEEE, 2010.

[20]   International Commission on Non-Ionizing Radiation Protection. "Guidelines for limiting exposure to time-varying electric, magnetic, and electromagnetic fields (up to 300 GHz)". *Health Phys.* 74 (4) (1998): pp. 494–522.

[21]   B. L. G. Jonsson, S. Shi, L. Wang, F. Ferrero, and L. Lizzi. "On methods to determine bounds on the Q-factor for a given directivity". *ArXiv e-prints* (2017).

[22]   E. Karipidis, N. D. Sidiropoulos, and Z. Q. Luo. "Far-field multicast beamforming for uniform linear antenna arrays". *IEEE Transactions on Signal Processing* 55 (10) (2007): pp. 4916–4927.

[23]   O. Kivekas, J. Ollikainen, T. Lehtiniemi, and P. Vainikainen. "Bandwidth, SAR, and efficiency of internal mobile phone antennas". *IEEE Transactions on Electromagnetic Compatibility* 46 (1) (2004): pp. 71–86.

[24]   N. Kuster and Q. Balzano. "Energy absorption mechanism by biological bodies in the near field of dipole antennas above 300 MHz". *IEEE Transactions on Vehicular Technology* 41 (1) (1992): pp. 17–23.

[25]   Z. Q. Luo, W. K. Ma, A. M. C. So, Y. Ye, and S. Zhang. "Semidefinite relaxation of quadratic optimization problems". *IEEE Signal Processing Magazine* 27 (3) (2010): pp. 20–34.

[26]   *Notice of inquiry.* Commission Documents 13-39. FCC, 2013.

[27]   *Notice of proposed rulemaking.* Commission Documents 15-138. FCC, 2015.

[28]   N. Ojaroudiparchin, M. Shen, S. Zhang, and G. F. Pedersen. "A switchable 3-D-coverage-phased array antenna package for 5G mobile terminals". *IEEE Antennas and Wireless Propagation Letters* 15 (2016): pp. 1747–1750.

[29]   N. Perentos, S. Iskra, A. Faraone, R. J. McKenzie, G. Bit-Babik, and V. Anderson. "Exposure compliance methodologies for multiple input multiple output (MIMO) enabled networks and terminals". *IEEE Transactions on Antennas and Propagation* 60 (2) (2012): pp. 644–653.

[30] T. S. Rappaport, S. Sun, R. Mayzus, H. Zhao, Y. Azar, K. Wang, G. N. Wong, J. K. Schulz, M. Samimi, and F. Gutierrez. "Millimeter wave mobile communications for 5G cellular: it will work!" *IEEE Access* 1 (2013): pp. 335–349.

[31] W. Roh, J. Y. Seol, J. Park, B. Lee, J. Lee, Y. Kim, J. Cho, K. Cheun, and F. Aryanfar. "Millimeter-wave beamforming as an enabling technology for 5G cellular communications: theoretical feasibility and prototype results". *IEEE Communications Magazine* 52 (2) (2014): pp. 106–113.

[32] T. Schmid, O. Egger, and N. Kuster. "Automated E-field scanning system for dosimetric assessments". *IEEE Transactions on Microwave Theory and Techniques* 44 (1) (1996): pp. 105–113.

[33] S. Shi, L. Wang, and B. L. G. Jonsson. "Antenna current optimization using SDR method". *IEEE Transactions on Antennas and Propagation* (to be submitted).

[34] A. M.-C. So, J. Zhang, and Y. Ye. "On approximating complex quadratic optimization problems via semidefinite programming relaxations". *Math. Prog.* 110 (1) (2007): pp. 93–110.

[35] I. Syrytsin, S. Zhang, G. Pedersen, K. Zhao, T. Bolin, and Z. Ying. "Statistical investigation of the user effects on mobile terminal antennas for 5G applications". *IEEE Transactions on Antennas and Propagation* (in press).

[36] B. Thors, D. Colombi, Z. Ying, T. Bolin, and C. Törnevik. "Exposure to RF EMF from array antennas in 5G mobile communication equipment". *IEEE Access* 4 (2016): pp. 7469–7478.

[37] B. Thors, A.Thielens, J. Friden, D. Colombi, C. Törnevik, G. Vermeeren, L. Martens, and W. Joseph. "Radio frequency electromagnetic field compliance assessment of multi-band and MIMO equipped radio base stations". *Bioelectromagnetics* 35 (4) (2014): pp. 296–308.

[38] P. Vainikainen, J. Ollikainen, O. Kivekas, and K. Kelander. "Resonator-based analysis of the combination of mobile handset antenna and chassis". *IEEE Transactions on Antennas and Propagation* 50 (10) (2002): pp. 1433–1444.

[39] B. Xu, K. Zhao, D. Sjöberg, Z. Ying, and S. He. "An examination of RF EMF exposure compliance of 5G user equipment using phased arrays at 15 GHz". *IEEE Antennas and Wireless Propagation Letters* (submitted for publication).

[40] B. Xu, K. Zhao, B. Thors, D. Colombi, O. Lundberg, Z. Ying, and S. He. "Power density measurements at 15 GHz for RF EMF compliance assessments of 5G user equipment". *IEEE Transactions on Antennas and Propagation* (submitted for publication).

[41] Z. Ying. "Antennas in cellular phones for mobile communications". *Proceedings of the IEEE* 100 (7) (2012): pp. 2286–2296.

[42]   S. Zhang, X. Chen, I. Syrytsin, and G. F. Pedersen. "A planar switchable 3D-coverage phased array antenna and its user effects for 28 GHz mobile terminal applications". *IEEE Transactions on Antennas and Propagation* (in press).

[43]   K. Zhao, Z. Ying, and S. He. "EMF exposure study concerning mmWave phased array in mobile devices for 5G communication". *IEEE Antennas and Wireless Propagation Letters* 15 (2016): pp. 1132–1135.

[44]   K. Zhao, C. Gustafson, Q. Liao, T. Bolin, Z. Ying, and S. He. "Channel characteristics and user body effects in an outdoor urban scenario at 15 and 28 GHz". *IEEE Transactions on Antennas and Propagation* (submitted to publication).

[45]   K. Zhao, S. Zhang, Z. Ying, T. Bolin, and S. He. "SAR study of different MIMO antenna designs for LTE application in smart mobile handsets". *IEEE Transactions on Antennas and Propagation* 61 (6) (2013): pp. 3270–3279.

[46]   K. Zhao, J. Helander, D. Sjöberg, S. He, T. Bolin, and Z. Ying. "User body effect on phased array in user equipment for 5G mmWave communication system". *IEEE Antennas and Wireless Propagation Letters* (in press).